Directed Energy Accelerated Lightsails

Giovanni Santi
Università di Padova, Centro di Ateneo di Studi e Attività Spaziali (CISAS), via Venezia, 15, 35131
https://orcid.org/0000-0003-2352-0976
Giulio Favaro
University of Padova https://orcid.org/0000-0002-0351-6833
Alain Jody Corso
Consiglio Nazionale delle Ricerche - Istituto di Fotonica e Nanotecnologie (CNR-IFN), via Trasea,7, 35131
Philip Lubin
Department of Physics, University of California - Santa Barbara, CA, 93106
Marco Bazzan
Università di Padova, Dipartimento di Fisica e Astronomia, via Marzolo 8, 35131
Roberto Ragazzoni
IstitutoNazionale di Astrofisica, Osservatorio Astronomico di Padova, Vicolo dell'Osservatorio, 5,35122
Denis Garoli
Istituto Italiano Tecnologie, Via Morego, 30 16163 Genova, Italy
Maria Guglielmina Pelizzo (pelizzo@dei.unipd.it)
Consiglio Nazionale delle Ricerche

Article

Keywords: Directed Energy Accelerated Lightsails, probe , deep space , ground-based large-aperture phased laser array

Posted Date: October 20th, 2021

DOI: https://doi.org/10.21203/rs.3.rs-943018/v1

Version of Record: A version of this preprint was published at Communications Materials on April 5th, 2022. See the published version at https://doi.org/10.1038/s43246-022-00240-8.

Directed energy accelerated lightsails

Giovanni Santi[a], Giulio Favaro[b], Alain J. Corso[c], Philip Lubin[d], Marco Bazzan[b], Roberto Ragazzoni[b,e], Denis Garoli[f], and Maria G. Pelizzo[g]

[a] *Università di Padova, Centro di Ateneo di Studi e Attività Spaziali (CISAS), via Venezia, 15, 35131 Padova, Italy*

[b] *Università di Padova, Dipartimento di Fisica e Astronomia, via Marzolo 8, 35131 Padova, Italy*

[c] *Consiglio Nazionale delle Ricerche - Istituto di Fotonica e Nanotecnologie (CNR-IFN), via Trasea, 7, 35131 Padova, Italy*

[d] *Department of Physics, University of California - Santa Barbara, CA, 93106*

[e] *Istituto Nazionale di Astrofisica, Osservatorio Astronomico di Padova, Vicolo dell'Osservatorio, 5, 35122 Padova, Italy*

[f] *Istituto Italiano Tecnologie, Via Morego, 30 16163 Genova, Italy*

[g] *Consiglio Nazionale delle Ricerche, Istituto di Elettronica, Ingegneria dell'Informazione e delle Telecomunicazioni, via Gradenigo, 6B, 35131 Padova, Italy*

Abstract

A lightsail accelerated via directed energy is a candidate technology to send a probe into the deep space in a time period compatible with human life. The light emitted by a ground-based large-aperture phased laser array is directed onto the lightsail to produce a thrust by transferring the momentum of the incident photons. To achieve high efficiency propulsion, the lightsail must be characterized by extremely low mass, high reflectance and minimal absorption in the Doppler-shifted laser wavelength range, while high emissivity in the infrared is required for thermal management. Optimized multilayer structures allow ultralight spacecraft being accelerated by laser radiation pressure up to 20% of the light velocity, and eventually even above, as long as a compromise between efficiency and weight is achieved. Key aspect is the ability to survive to the temperature increase during the acceleration phase, which can be fateful for the system.

---

1 Introduction

Space exploration is an objective of fundamental importance for the economic, social and, above all, cultural growth of the society. In the incoming years, new technologies and missions will be devoted to the exploration of the solar system and to the colonization of nearby space. On the other hand, exploration of the deep space still remains an impractical dream, mainly due to the limited propulsive means. However, more and more researchers, driven by the desire for knowledge of the universe, are orienting their activities towards the search for technological solutions. Recently, attention is

paid in evaluating two possible technologies, being nuclear and laser propulsion, which in principle could allow interstellar travels. Nuclear propulsion is considered the most promising technology, even though practical and cost-effective solutions have not been identified yet. The main problems relate to the large mass of propellant involved in ground preparation, which can pose risks for human health. An alternative solution is represented by the use of a directed energy (DE) system, such as sails accelerated by the radiation pressure of a light beam.

Solar sails have been developed and tested on various missions starting from the 2010 [1]; however, the isotropic power provided by the Sun is not enough to allow the acceleration needed to reach the desired relativistic velocity in the target distance, so that high power lasers are now considered as potential source of radiation. Depending on the mechanisms that generate the thrust, laser propulsion systems can be either propellant-based or propellant-less [2]: in the first case a thrust is provided by the light driven ejection of a flux of ablated particles of non-zero rest mass [3, 4], while for the second one the primary mechanism of thrust generation is due to the energy transfer from incident photons [5, 6, 7, 8, 9]. Moreover, a new process which generates propulsion has been recently discovered, being the light-induced ejected electrons (LIEE) in graphene materials [10]. An additional concept refers to the use of the laser for on-board conversion of the beamed energy into electricity used to power an electric propulsion system [11]. While useful for high mass missions in the solar system, neither of these "mass ejection" techniques are designed for nor capable of achieving relativistic speeds.

The main advantage in using the DE propellant-less approach is that source of energy is fully external to the spacecraft itself, so that there is no need to carry additional weight. Moreover, a ground based laser system could be re-used to launch multiple spacecrafts, making its realization cost effective. The goal of the NASA Starlight program [12] is to enable small spacecraft to achieve relativistic flight, in order to plan the first interstellar missions with targets including our nearest neighbor, the Alpha Centauri system [7, 8, 9]. This line of thought was subsequently continued by the Starshot Breakthrough Initiative [13]. In both the NASA Starlight and subsequent Starshot programs the spacecraft system consists of two main components: a primary spacecraft reflector, or *"lightsail"*, propelled by a phased array laser, and a small payload, called a *wafer scale spacecraft or starchip*, that contains all the electronic components and sensors to gather and transmit the information. A hybrid mode of combining the spacecraft and reflector into a quasi-homogeneous structure is also conceivable. This study is agnostic to the detailed approach. As the laser flux at the spacecraft reflector is of the order of 10-100 GW/m^2 at distances from the laser typically of order the distance to the Moon, a laser phased array based is used in place of one single high powerful laser [9]. The NASA Starlight and DEEP-IN programs explored this extensively in a series of papers and laboratory demonstrations. Prototypes supporting phase locking over array diameters up to 50 km, were feasible with better than 1/100 of a wave phase error achieved [12], exceeding the previous expectations. This is extremely encouraging, though a vast amount of technological development needs to be done to realize such a system. The use of phased laser array would reduce the overall complexity of the

source development project, allowing the modularity needed to laboratory prototyping engineering and relative tests.
The present study assumes a scalable, modular DE source with emission at 1064 nm, used to accelerate a spacecraft up to a target velocity of 0.2c; this value could be further extended depending on the requirements of the mission. Such laser wavelength has been proposed and demonstrated in the NASA Starlight program using Yb doped fiber laser amplifiers in a MOPA (Master Oscillator Phased Array) topology. The optimization at a selected wavelength is only one example and does not exclude any other one. Since one of the goals is to allow relativistic flight, the high speed spacecraft will experience a longer wavelength than was initially emitted and thus two options need to be explored. One is that the laser changes its emission wavelength to shorter ones as the spacecraft speeds up, so that the received wavelength at the spacecraft is constant, or the reflector needs to be broadband enough to allow a modest or perhaps large dynamic range of received wavelengths. This paper focuses on the latter approach and looks at relatively broad bandwidth reflectors. It outlines the criteria to select the laser wavelength through a detailed analysis of the materials thermal properties, being generally more suitable as the wavelength increases, and modelling the ligthsail thermal evolution; vice-versa, after selecting the laser operation wavelength, the lightsail's structure should be engineered to survive to the extreme conditions arising during the acceleration phase.
In this perspective, the aim of this work is to provide a step ahead to the analysis reported by Ilic et al. [14]. In that paper, the authors demonstrated the feasibility of using ideal thin-film heterostructures as building-block elements of a laser-driven lightsail at 1200 nm, due to their ability to achieve substantial reflectance while maintaining low absorption in the near-infrared, significant emissivity in the mid-infrared, and a very low mass. They provided a minimization of a figure of merit which describes the lightsail performance as function of its structural parameters. In some cases, they have also evaluated the solution in term of their thermal stability assuming a strict thermal equilibrium. In the present work, real periodic multilayer structures undergo an optimization process at 1064 nm, by including the contribution of the lightsail's material absorption. The thermal analysis is carried on afterwords by providing an accurate description of the thermal evolution as a function of the spacecraft's velocity in non-thermal equilibrium. In doing so, we assume a set of extinction coefficient values in the Doppler-shifted wavelength region of the laser source to evaluate the dependence on the final temperature, together with different condition of the DE laser power. Lightsail optimization was carried out considering a series of multilayers that include different materials. We finally discuss the impact of the laser wavelength selection in the propulsion system definition and some suitable structures to be used, which guarantee survival of the lightsail during the acceleration phase at 1064 nm, as well as their associated manufacturing challenges.

2 Optimization of the multilayer lightsail

The lightsails are realized by considering a material couple arranged in a stack of N layers, as represented in Figure 1. In this description D is the characteristic dimension of the sail and α models its specific shape, such that the sail surface is $S = \alpha D^2$.

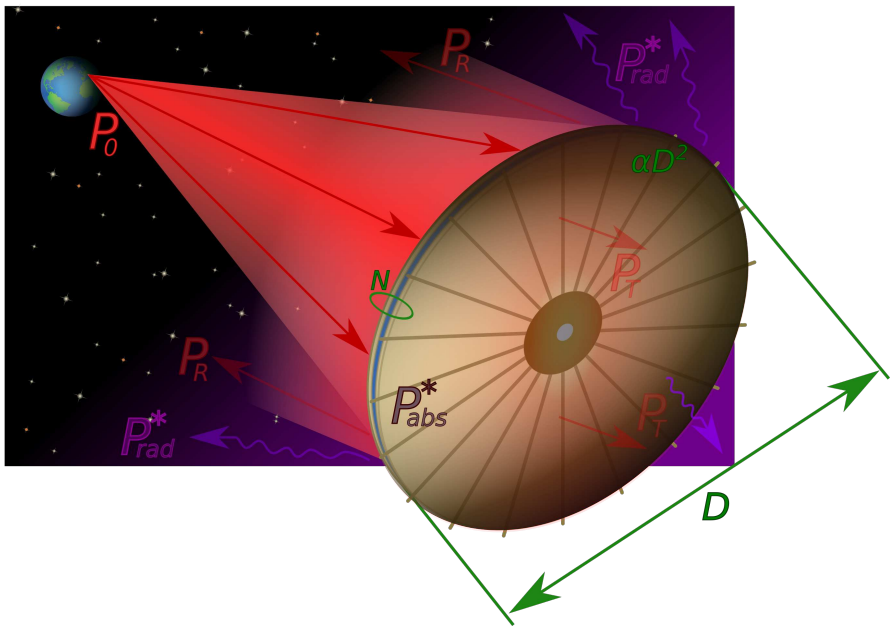

Figure 1: Representation of the operation conditions of the multilayered lightsail. The red arrows denote the incident, transmitted and reflected laser power, while the violet ones indicate the thermal radiation leaving the structure from the front and back surfaces. The surface area is modelled as αD^2; $\alpha = 1$ for a squared lightsail of side D and $\alpha = \pi/4$ for a circular lightsail of diameter D.

Optimization of the lightsail requires the correct determination of the equation of motion of the object under the trust provided by the laser beam. Assuming that the laser system provides a constant beam power P_0 at all distances and settings, the power of the incident beam on the lightsail as a function of the spacecraft speed $\beta = v/c$ and as seen by the reference frame from Earth is $P_0(1-\beta)$, where the term $(1-\beta)$ accounts for the photon travel time between the beamer and the lightsail. Depending on the lightsail's properties, the incident power is either reflected, transmitted or absorbed. The interaction of laser photons can be thus modelled by accounting for the optical coefficients and for the Doppler transformation of the incident power (see Supplmentary Information, Section 1). By introducing the reflectance R, transmittance T and absorption A, calculated at the corresponding Doppler shifted wavelength as seen by the sail, and considering that the variation of the energy of the spacecraft is equal to the difference between the power impinging on the ligthsail and that lost by transmittance and reflectance, the following differential can be obtained:

$$\mathrm{d}t = \frac{mc^2\gamma^3}{P_0}\frac{(1+\beta)}{(1-\beta)}\frac{1}{[\mathrm{A}+2\mathrm{R}]}\mathrm{d}\beta; \tag{1}$$

Note that Equation (1) is formally equivalent to that obtained in [7], [14], [15], with the difference that the contribution for absorption is now included. The acceleration distance at the end of the acceleration phase $L(\beta_f = 0.2)$ is used to determined the point where the diffraction spot from the laser beamer is equal to the dimension of the sail [14] by integrating the instantaneous speed from 0 up to the target velocity β_f in Equation (1). By writing explicitly the mass term $m = m_s + m_p = \alpha D^2\rho_s + m_p$, where m_s is the mass of the sail, m_p the mass of the payload and ρ_s the area density, it is then possible to derive an expression for the requirements on the laser system $P_0 d_0$, where d_0 is the diameter of the beamer. According to [7], the maximum speed occurs when $m_s = m_p$, so that:

$$P_0 d_0 = 4\lambda_0 c^3\sqrt{m_p}\sqrt{\alpha}\int_0^{\beta_f}\frac{\sqrt{\rho_s}}{[\mathrm{A}+2\mathrm{R}]}\frac{\beta\gamma}{(1-\beta)^2}\mathrm{d}\beta = 4\lambda_0 c^3\sqrt{m_p}\sqrt{\alpha}\cdot FOM(\rho_s, \mathrm{R}, \mathrm{A}) \tag{2}$$

where the function $FOM(\rho_s, \mathrm{R}, \mathrm{A})$ is the Figure of Merit (FOM) to be optimized in this problem [14] in order to minimize the beamer specifications. The FOM allows, indeed, to ignore the payload mass while comparing different sail structures as it includes only ρ_s, and at the same time poses a constraint on the characteristics of the beamer.
The materials considered for the multilayer ligthsail optimization are Si, MgF_2, SiC, SiO_2, Al_2O_3, and TiO_2. These materials are in fact widely used in the realization of optical mirrors and filters for different purposes, so optical parameters are available in literature; moreover, with respect to other common materials such as ZrO_2 and Ta_2O_2, they have lower densities, which makes them more suitable candidates for the ligthsails. A genetic algorithm is applied to obtain the optimized layer thicknesses by minimizing the FOM in (2). The optical constants of the materials used for the computation of the FOM are taken from the literature [16, 17, 18, 19, 20, 21, 22, 23, 24] and reported in Figure 1 and 2 in the Supplementary Information. Note that while the real part of the refraction index is available for all the materials in the thin film form, the extinction coefficient barely impact on the FOM value; when not available, as in the case of Si and $Al2O3$, they have been borrowed from those determined on crystal bulks and carefully used in the thermal analysis (see Section 3); moreover, it has been verified that the real part of the refraction index of Si and $Al2O3$ in amorphous and crystal form are very similar. Firstly, we simulate stacks which include one of the selected materials coupled with the vacuum (VU). This allows to obtain ideal structures with a maximum optical contrast and thus upper bound performance. As a second step different materials combinations have been considered. The optimization is carried out for different number of layers (up to 7). The obtained FOM are reported in Figure 2a and Figure 2b, respectively. Interestingly, a decreasing trend as the number of layers increases is observed in the FOM value of SiO_2, Al_2O_3 and MgF_2 based structures in Figure 2a, being the Si-based structures the optimum ones, while an opposite behaviour is observed for the

real structures as reported in Figure 2b. When the layer number is increased from an even number to an odd one, the FOM value is almost unchanged, even when a large number of layers are used. By looking to Table 1, where the parameters of the structures are reported, it is clear that the optimization of the even structures lead always to a last layer with a thickness of 10 nm, which has been set as the minimum acceptable by the algorithm. This means that, in the even structures, the increase of the last layer thickness always degrade the FOM values. Moreover, the optimal structures are represented by the odd ones with the lower adjacent number. In particular, the structures $N = 1, 3$ have the lower FOM values, while the $N = 2, 4, 6$ are considered as a worsening case of those with $N = 1, 3, 5$ in term of propulsion efficiency, as the additional top layer always increased the FOM.
Single layer structures with minimum FOM values are those built by materials characterized by an higher refractive index, being the case of Si, SiC and TiO_2. These materials are thus selected as the base ones for building more complex structures. The material that in principle should be used as a second layer in a bi-layer or, more in general, in a multilayer is SiO_2, as when coupled with each of the base materials provides the best performance in term of FOM (Table 1); however, in the next section, it will be clear that even layer structure can be only slightly beneficial for the thermal stability of the structure, while, as said, are detrimental for the FOM.
Two parameters concur to determine the FOM value of the multilayers, i.e. the reflectance and the areal density, this last can be calculated as $\rho_s = \sum_i \rho_i t_i$, where ρ_i is the mass density of the i-th layer with thickness t_i, being the first layer eventually the substrate. In Table 1 such parameters are reported for each of the 1, 2, 3, 4-layers stack considered. Note that, for a given N, the structures having lower ρ_s, are generally associated with a lower FOM value, in accordance with our analysis. In Figure 3 the areal density, the reflectance and FOM of selected structures are reported to allow a comparison of their performance.

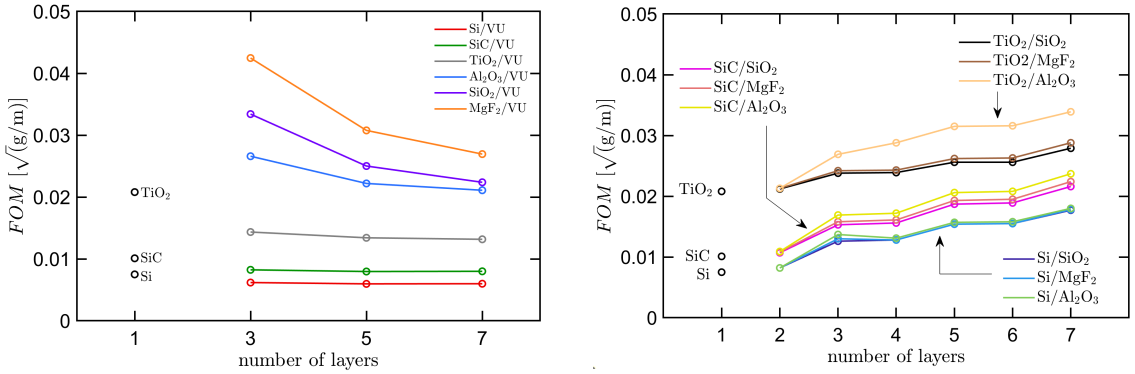

Figure 2: Optimized FOM values from different multilayer. Figure 2a: structures based on material$_1$/VU. Figure 2b: structures based on material$_1$/material$_2$. The simulations are performed for an increase number of layers N.

Structure	ρ [g/cm^3]	t$_{opt}$ [nm]	ρ_s [g/m^2]	FOM [$\sqrt{g}/m$]
Si	2.33	52	0.135	0.0074
SiC	3.24	61	0.198	0.0101
TiO_2	4.23	104	0.440	0.0208
Al_2O_3	3.95	157	0.6202	0.0509
SiO_2	2.65	181	0.480	0.0736
MgF_2	3.15	188	0.592	0.0965
Si/SiO_2	2.33/2.65	56/10	0.157	0.0082
Si/MgF_2	2.33/3.15	57/10	0.164	0.0083
Si/TiO_2	2.33/4.23	55/10	0.170	0.0085
Si/Al_2O_3	2.33/3.95	57/10	0.172	0.0085
SiC/SiO_2	3.24/2.65	64/10	0.234	0.0107
SiC/MgF_2	3.24/3.15	63/10	0.236	0.0108
SiC/Al_2O_3	3.24/3.95	63/10	0.244	0.0109
SiC/TiO_2	3.24/4.23	60/10	0.237	0.0108
TiO_2/SiO_2	4.23/2.65	102/10	0.458	0.0212
TiO_2/MgF_2	4.23/3.15	103/10	0.467	0.0213
TiO_2/Al_2O_3	4.23/3.95	101/10	0.467	0.0214
$Si/SiO_2/Si$	2.33/2.65	88/96/89	0.668	0.0126
$SiC/SiO_2/SiC$	3.24/2.65	85/142/88	0.937	0.0153
$TiO_2/SiO_2/TiO_2$	4.23/2.65	121/203/121	1.562	0.0238
$Si/SiO_2/Si/SiO_2$	2.33/2.65	89/97/87/10	0.694	0.0128
$SiC/SiO_2/SiC/SiO_2$	3.24/2.65	98/113/97/10	0.958	0.0156
$TiO_2/SiO_2/TiO_2/SiO_2$	4.23/2.65	121/205/117/10	1.5765	0.0239

Table 1: Parameters of optimized structures: volume density ρ, optimized thickness t_{opt}, area density ρ_s and FOM.

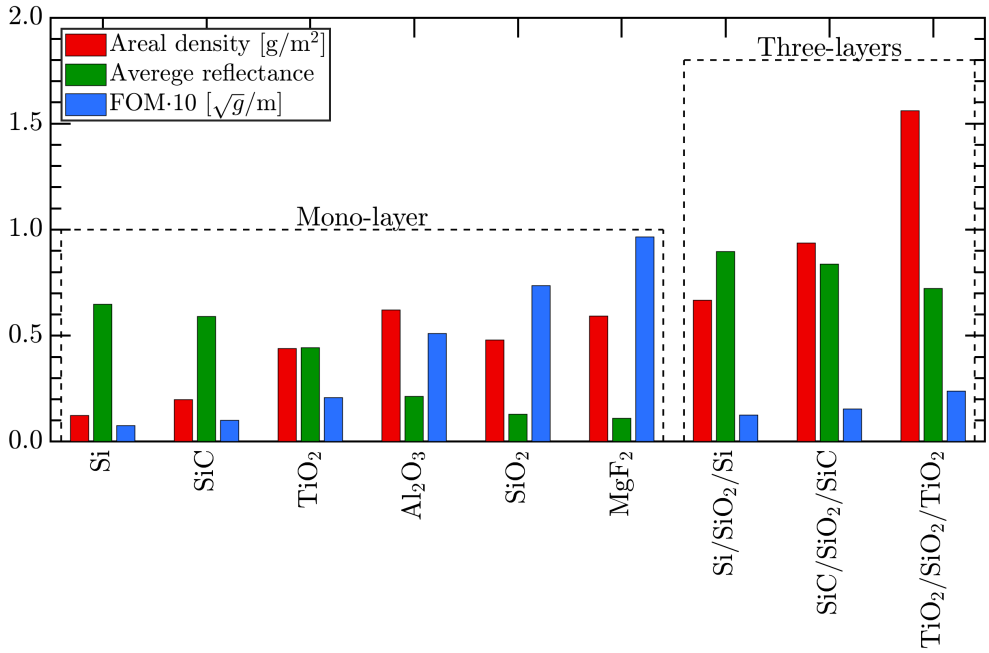

Figure 3: Areal density (red bar) and (average) reflectance (green bar) of selected lightsail structures considered, as grouped by the number of layer. For each group, the value of the FOM increases from left to right.

The acceleration time to reach the final velocity β_f can be computed by integrating equation (1):

$$t = \frac{2\rho_s c^2}{I_0}\left[\int_0^{\beta_f} \frac{\gamma}{(1-\beta)^2[\mathrm{A}+2\mathrm{R}]}\cdot \mathrm{d}\beta\right] = t_c \cdot \xi \tag{3}$$

In the optimal mass regime (i.e. $m_s = m_p$), in (3) m has been re-written as $m = 2\cdot S\cdot\rho_s$, while $P_0 = S \cdot I_0$. Consequently, the equation is independent on the sail surface area, while it depends on the irradiance I_0. In (8), t results as a product of two terms, the *characteristic time* of the system $t_c = \frac{2\rho_s c^2}{I_0}$ and the dimensionless term ξ that takes into account the relativistic efficiency of the lightsail. The second term, ξ, depends on the optical properties of the lightsail and it reaches its minimum value of 0.1261 in the case of a perfectly reflective lightsail (i.e. R=1 and A=0 at all velocities). Note that the equation (3) is formally equivalent to the one provided by Kulkarni et al. [8], except for the fact that in this case the lightsail is not a perfect reflector.
Figure 4 shows the acceleration time in the beamer reference frame for the 1- and 3-layer lightsail structures considered in this study. As expected, the minimum time is associated to the Si-based structures, which have the minimum FOM values, while the higher value are for the TiO_2-based structures. Given an irradiance I_0, structures with lower ρ_s have also a smaller characteristic time. However, given a payload of mass m_p, the ratio m_p/ρ_s determines the lightsail's area S, so that structures having lower

area density imply lightsails of larger size. For example, a payload of 1 gram requires requires a sail of $S \approx 1.5$ m^2 in the case of the $Si/SiO_2/Si$ structure, while only of $S \approx 0.6$ for the $TiO_2/SiO_2/TiO_2$ one. We can conclude that couples with high optical contrast results in thinner layers, with a diminishing of the areal density, and ultimately an increasing of the propulsion efficiency. By looking at the results obtained so far, it appears that the optimum solution are given by the single layer of Si (target velocity achieved after 4336 s for $I_0 = 1$ GW, 433 s for $I_0 = 10$ GW, 43 s for $I_0 = 100$ GW) and SiC (target velocity achieved after 7372 s for $I_0 = 1$ GW, 737 s for $I_0 = 10$ GW, 74 s for $I_0 = 100$ GW). However, in the next section the analysis carried out on the thermal stability of such structures will demonstrate their instability, and prove that the TiO_2 based structures are those to be further considered. With a single layer structure, the target velocity is achieved after 22658 s for $I_0 = 1$ GW, 2266 s for $I_0 = 10$ GW, 227 s for $I_0 = 100$ GW, while with the $TiO_2/SiO_2/TiO_2$ in 49122 s, 4912 s and 491 s respectively.

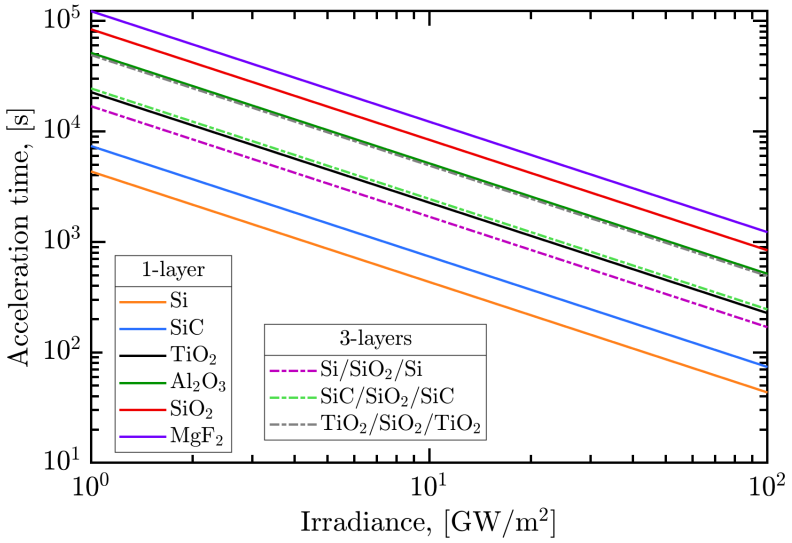

Figure 4: Acceleration time to reach β_f in the beamer reference frame for the lightsail structures considered in this study.

3 Thermal stability of the lightsail

The lightsail thermal analysis of the sail is of upmost importance to understand whether the chosen structure will survive the acceleration process. Energy flows inside the system through the absorbed power and it leaves the system via the radiated power. The absorbed power in the sailcraft reference frame (identified by an *) can be expressed as:

$$P^*_{abs} = I_0 S \frac{1-\beta}{1+\beta} \mathrm{A}(\lambda_0, \beta) \tag{4}$$

Since the lightsail is a pure passive device, the emitted power P^*_{rad} is modeled by means of thermal radiation theory:

$$P^*_{rad} = S \cdot \int_\lambda \varepsilon_\lambda(\mathrm{T}^*, \lambda) \cdot \mathrm{E_{b,\lambda}}(\mathrm{T}^*, \lambda)\mathrm{d}\lambda \tag{5}$$

being ε_λ the *spectral hemispherical emissivity* and $E_{b,\lambda}$ the *spectral blackbody emittance*. The net power is computed by the difference between the absorbed and radiated ones from equations (4) and (5) respectively. Differently from previous analysis [14], the temperature is then calculated using the thermal energy absorbed in the system in non-equilibrium conditions. Results will be remarkably important to assess the thermal evolution and stability of the ligthsail.
The time-dependent temperature evolution is obtained though numerical calculations based on the following non-linear non-homogeneous equation:

$$\frac{\partial T^*}{\partial t^*} = \frac{P^*_{abs} - P^*_{rad}}{C_{sail}} \tag{6}$$

where $C_{sail} = \sum_i m_i c_i$ is the heat capacitance of the lightsail as given by the sum of the contribution of the i-th thin film of mass m_i and specific heat capacity c_i. In our calculation, we have taken into account the dependence of C_{sail} by the temperature through β. By operating the change of variable $t^* = t\gamma^{-1}$, which relates the proper time of the beamer with the one of the sail, in (1), $\mathrm{d}t^*$ can be express in term of $\mathrm{d}\beta$:

$$\mathrm{d}t^* = \frac{2\rho_s c^2 \gamma}{I_0} \left[\frac{(1+\beta)}{(1-\beta)} \frac{\gamma}{[\mathrm{A} + 2\mathrm{R}]} - \beta \left(\int_0^\beta \frac{\gamma(y)}{(1-y)^2} \frac{1}{\mathrm{A} + 2\mathrm{R}} \, \mathrm{d}y \right) \right] \mathrm{d}\beta \tag{7}$$

The right term of (6) linearly depends on the area of the lightsail S through the net power $P^*_{abs} - P^*_{rad}$; at the same time, the heat capacitance scales linearly with the area through the system mass m, so that $C_{sail} = 2 \cdot S \cdot \sum_i \rho_i t_i c_i$; hence, the thermal balance of the lightsail is independent on its surface area. The acceleration and the thermal evolution of the system thus depends only on the irradiance I_0.
At each integration step $\mathrm{d}\beta$, the $\mathrm{d}t^*$ retrieved by equation (7) is used to calculate the difference between the absorbed and emitted power in order to determine the temperature increment for subsequent iterations. To perform such computation, a precise knowledge of the refractive index of the involved materials is required. While the real part is generally well known, the extinction coefficients is barely available in the full spectral range needed to make the thermal analysis and, when available, this is typically known with low accuracy. Therefore, while emittance calculations are performed assuming tabulated k in the range $\lambda = 1.5 - 50$ μm, which includes a $\sim 97\%$ of the power emitted by a body at 300 K and a $\sim 89\%$ of a body at 1500 K (see Figure 3 in the Supplementary Information), for the absorbed power in the laser Doppler range $\lambda = 1 - 1.225$ μm different values for the extinction coefficient have been considered, as these are critical for the thermal balance. In Figure 2 and 3 of the Supplementary Information some available k data from literature used in simulation are reported. Dielectric

materials such as TiO_2 and SiO_2 are high-temperature low-loss transparent materials, so that they can sustain higher temperatures more easily. In turn, semiconductor material such as Si and SiC can easily achieve extinction coefficient values of the order of $10^{-9} - 10^{-10}$ above the band-gap, but the value at the band-gap is temperature dependent and the absorption rapidly increases with the temperature. This can be a major issue if the band-gap falls in the Doppler-shifted wavelength range of the incident laser radiation. SiC has a very high absorption at 1064 nm and simulations show that this leads to a thermal instability of the lightsail even for low irradiance I_0 values, so that structures including this material have been discarded. In the case of Si, the experimental values of k, largely reported in literature, decrease as the wavelength increase [21],[25]. Unfortunately, the 1064 nm laser wavelength still falls within the absorption gap of the Si, so that it is foreseen that also this materials will not perform well in term of thermal stability. To prove so, a linear fit of the k data reported in Figure 3 of the Supplementary Information have been used in order to obtained values at each proper Doppler λ, each of which correspondent to a β along the acceleration phase, to perform thermal evolution simulations. Moreover, values scaled of one and two decades have been also used in simulations. For SiO_2 and TiO_2 the simulations assumed k values reported in literature, which are 10^{-7} [16] and $6 \cdot 10^{-5}$ [23] respectively, being these constant over the whole Doppler-shifted spectral range. However, simulation have been performed using even more optimistic values, as it is reasonable to assume that lower k can be achieved by engineering such materials.

Thermal evolution of selected stacks as function of β are reported in Figure 5, for the case of irradiance $I_0 = 1$ GW/m^2 and initial temperature $T = 50$ K. This values can resemble the case in which the lightsail is accelerated from outside the atmosphere. While the most performing solution in term of FOM is the Si single layer, this actually results thermally unstable even for very low k values (Figure 5a). On the contrary, the TiO_2 single layer shows remarkable thermal stability for low k values (Figure 5b). Simulation have been performed also in order to verify if a TiO_2 capping layer deposited on a Si layer can stabilize the sail; results show that this is the case only for the lower silicon k values. For this reason, structures based on Si are not further investigated. On the contrary, TiO_2 coupled with SiO_2 structures have been deeply analyzed. The use of a multilayer in place of a single layer can offer some advantages is in term of the maximum temperature achieved, which decrease if 3 (Figure 5c) or more layers are used, but only for high k value of TiO_2 (Figure 6). However, as the number of layers increase, the FOM increase too, so that it is not convenient to use more then 3 layers, unless the total thickness of the structure matter in term of mechanical stability. In fact, while the single layer thickness is of only 104 nm and the three layer one is 445 nm, the seven layers one reaches about 1.1 μm.

The results obtained so far highlight the role of TiO_2 in the thermal re-emission, which derives from the high values of k that characterized it over the whole IR range considered up to 50 μm. It is worth to note that the starting temperature does not affect the thermal evolution of the structure. As an example, in Figure 7 the case of a single TiO_2 layer with a $T_0 = 300$ K is reported to envision the case in which the ligthsail is

accelerated from ground. Clearly, the final temperature reached by the lightsail is the same of that reached with $T_0 = 50$ K, thus being independent from the starting one. Note that the TiO_2-based structures are also able to withstand an irradiance of $I_0 = 10$ GW/m^2 (Figure 8) and even $I_0 = 100$ GW/m^2 (Figure 9), as long as the the extinction coefficient do not exceed 10^{-7} and 10^{-8} respectively.

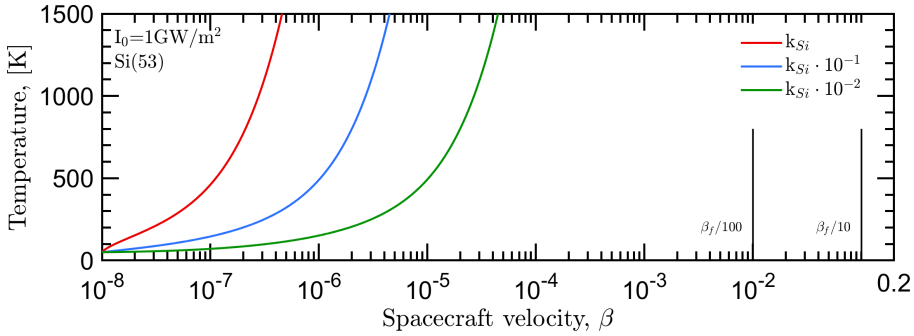

a

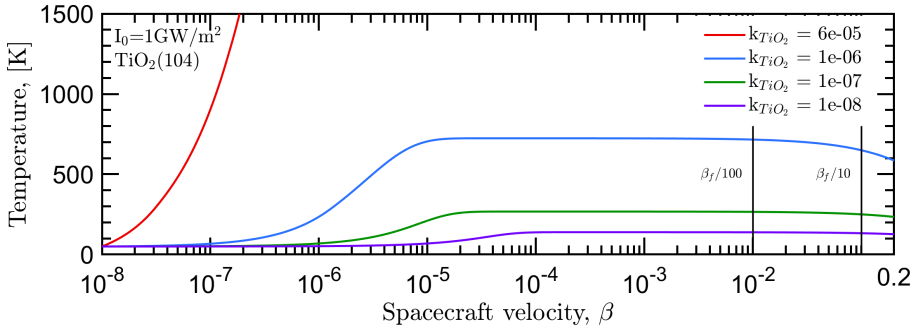

b

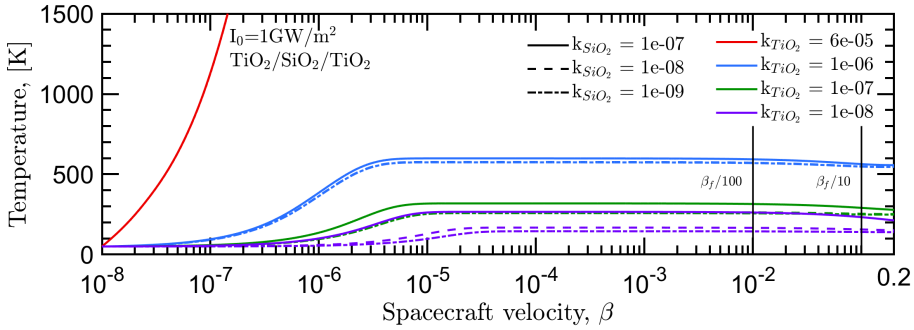

d

Figure 5: Temperature evolution of the Si single layer (a), of TiO_2 (b) single layers, and of $TiO_2/SiO_2/TiO_2$ tri-layer (c) lightsails for different values of the extinction coefficients, given a starting temperature T_0=50 K. Here the irradiance is $I_0 = 1$ GW/m^2.

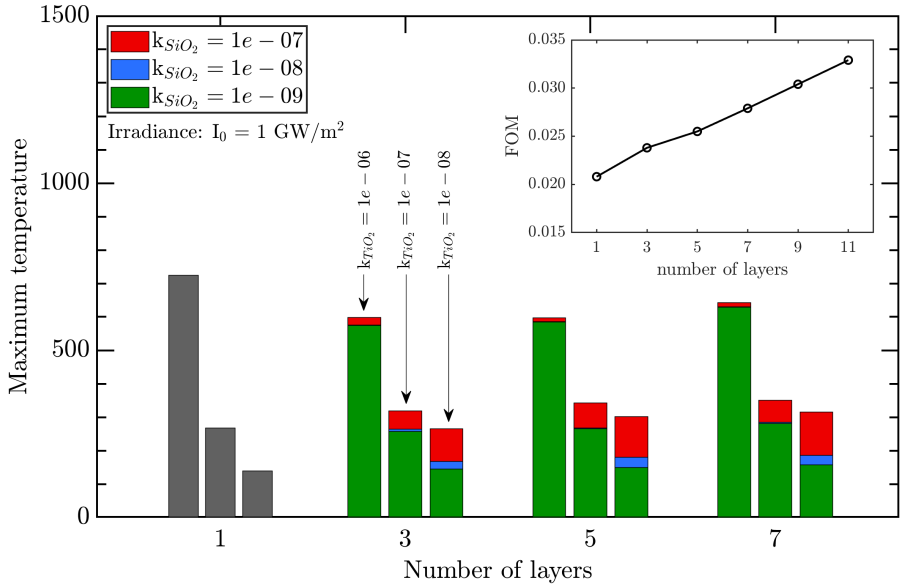

Figure 6: Maximum temperature reached during the acceleration phase by the TiO_2- based lightsail with SiO_2 as low-index material. The temperature is provided for different values of extinction coefficients. In the Inset the FOM is reported for increasing number of layers.

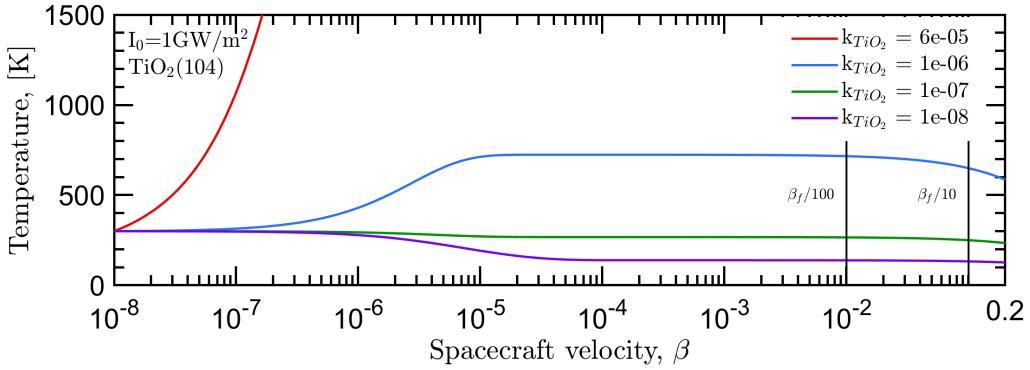

Figure 7: Temperature evolution of the TiO_2 single layer lightsail for different values of the extinction coefficients given a starting temperature T_0=300 K. Here the irradiance is $I_0 = 1$ GW/m^2.

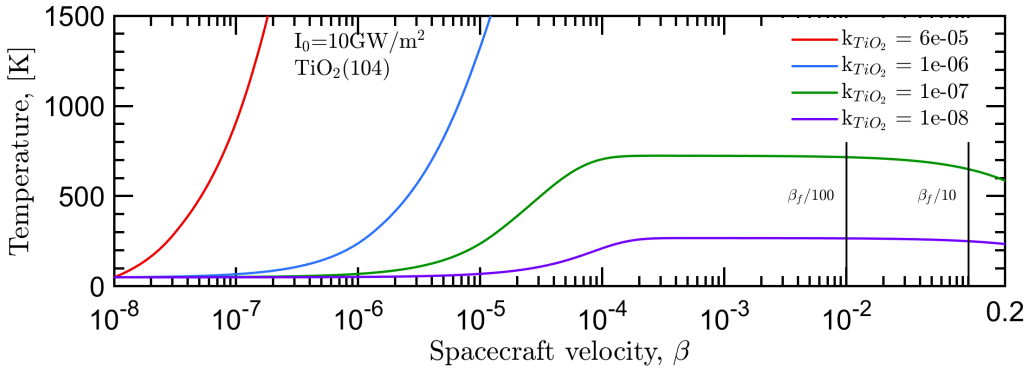

a

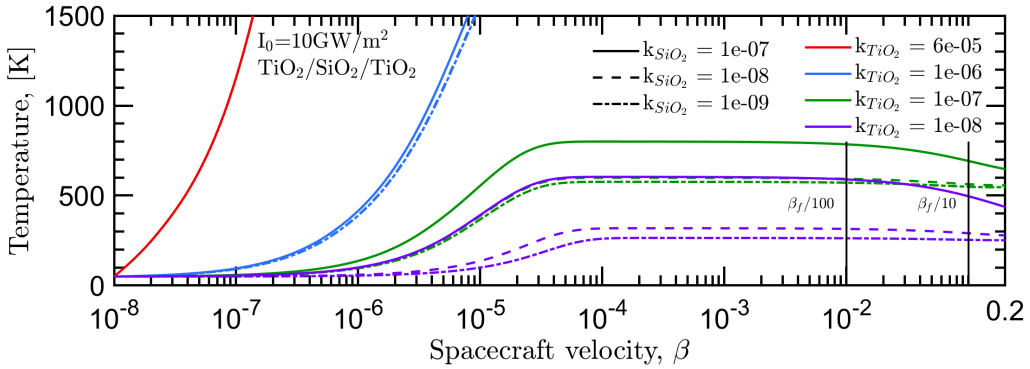

b

Figure 8: Temperature evolution of the TiO_2 monolayer (a) and of the $TiO_2/SiO_2/TiO_2$ trilayer (b) lightsails for different values of the extinction coefficients, given a starting temperature T_0=50 K. Here the irradiance is $I_0 = 10$ GW/m^2.

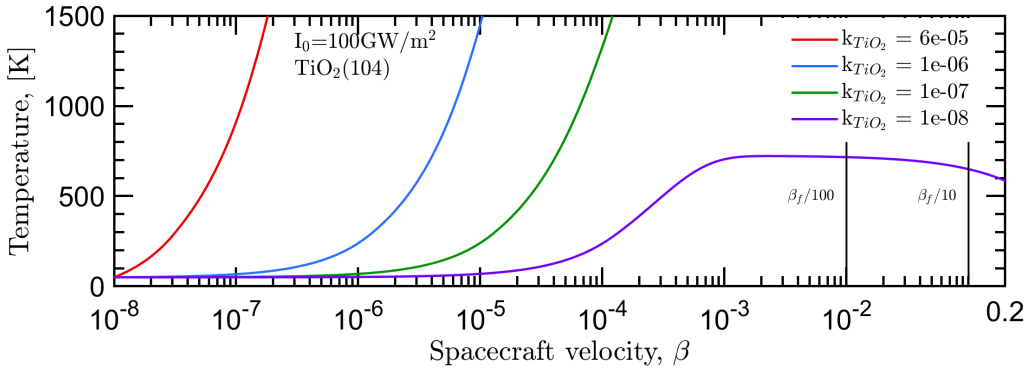

c

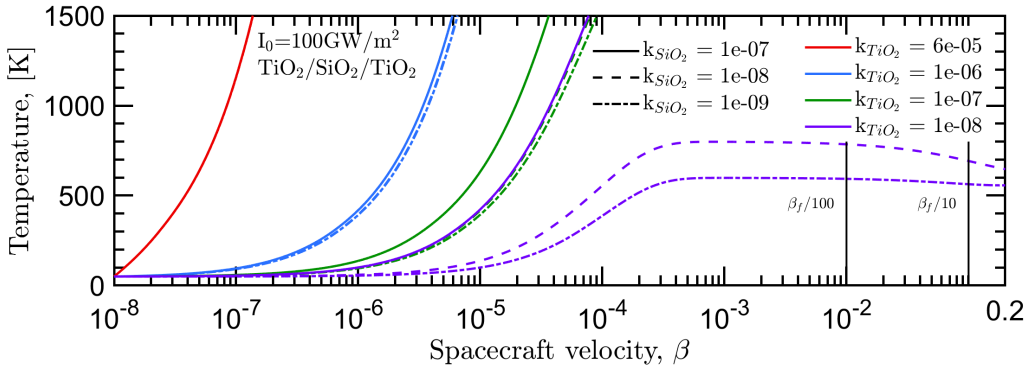

b

Figure 9: Temperature evolution of the TiO_2 monolayer (a) and $TiO_2/SiO_2/TiO_2$ tri-layer (b) lightsails for different values of the extinction coefficients, given a starting temperature T_0=50 K. Here the irradiance is $I_0 = 100$ GW/m^2.

4 Discussion and fabrication challenges

While the optimization of the FOM provide the structure which best perform in term of efficiency, the thermal analysis lastly states the feasibility of the experiment. In fact, from the results obtained in the previous section assuming the use of a 1064 nm laser source, the most suitable structure to be adopted are not the best in term of efficiency, but those capable to survive the journey, in particular those involving TiO_2 layers. However, to achieve such a challenging outcome, a major effort is needed to engineer the material in order to reduce the k in the laser Doppler wavelength range in order to allow the use of powers up to 10 GW and eventually 100 GW, with consequent reduction of the acceleration times shortening to 2266 and 227 s respectively. In addition, as the absorption coefficient of Si decreases at long wavelengths, the use of an operating wavelength above 1064 nm could be an advantage in terms of lightsail thermal stability and overall for the efficiency of the propulsion system. For example, the use of Yb-Er laser at 1.3 μm could guarantee higher lightsail performance, still combined with good transmittance in the atmosphere H-band.

In addiction to the theoretical analysis and possible lightsails design presented in previous sections, some practical considerations should be taken into account in relation of some of the most critical aspects of such an ambitious project. In particular, the extreme constrains on the mass requires all materials to be in thin film form. Therefore, the use of a thick substrate has to be excluded, while the self-standing solution represents the optimum solution, which can better resemble the results obtained with our simulations. However, this can pose some questions on the manufacturing process and mechanical stability, the last being discussed in the following. As an alternative, membranes could be used as substrates. High-performance, lightweight, and flexible materials that can meet the high-temperature requirements have been recently proposed. For example, fabrication of 44 mg/m^3 [26] and even 27.34 mg/m^3 [27] have been reported, with the possibility of peeling transparent single-layers fibrous membranes. The extremely low density is achieved by electro-spinning, which allows to obtain a very high porosity of the substrate membrane. The typical applications for such membranes are efficient heat insulation, acoustic absorption, water purification and many others [28], nevertheless they shares many of the characteristics that are desirable for our lightsails and can then be a promising solution that need further investigations. In particular, the effect of the membrane on the efficiency should be evaluated, even though probably limited. On the good side, deposition of thin film multilayer with meters scale area are already feasible by using physical vapour deposition processes.

Another aspect to be considered is the mechanical strength of the multilayer lightsail. There is very little information in the literature on the mechanical properties of thin films [29], though we can derive some general conclusions for our problem. To avoid a mechanical failure, the pressure acting of the lightsail must verify the condition:

$$P < (\sigma_{UTS} \cdot t)/D \tag{8}$$

where σ_{UTS} is the ultimate tensile strength of the sail material and t its thickness. The

instantaneous pressure P can be expressed by normalizing the force F acting on the lightsail to its surface S:

$$P = \frac{I_0}{c}\frac{1-\beta}{1+\beta}[(1+\beta)A + 2R] \tag{9}$$

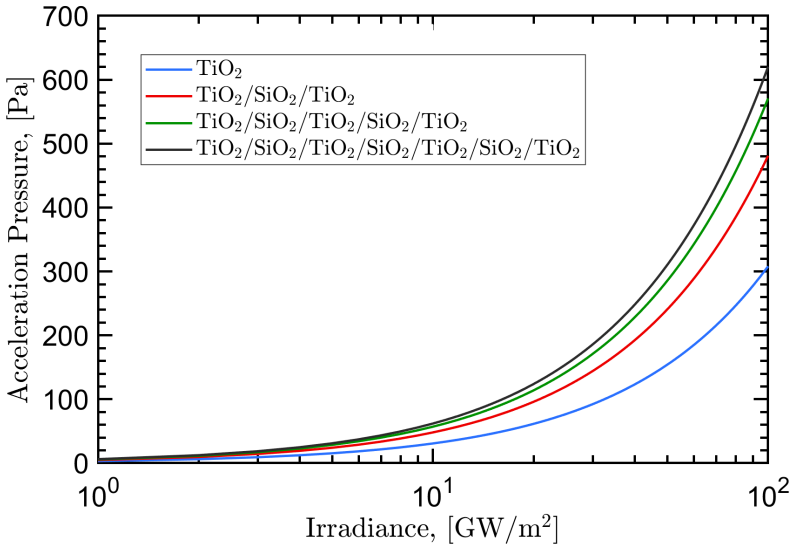

Figure 10: Maximum acceleration pressure to reach β_f in the beamer reference frame for the TiO_2-based lightsail structures considered in this study computed for different irradiance.

Figure 10 shows the maximum pressure experienced during acceleration by different TiO_2/SiO_2 -based multilayer lightsail, being the number of layers in the range between 1 to 7. In the most critical case of an irradiance of $I_0 = 100$ GW/m^2, the maximum pressure experienced increases from 308 Pa (single layer) up to 620 Pa (7-layers). Using Eq. 8, such value corresponds to a maximum ratio σ_{UTS}/D of 2.96 GPa/m for the single layer and 284 MPa/m for the 7-layers structure. While the σ_{UTS} for TiO_2 is not available at our knowledge, and more in general very limited information are available for amorphous materials, the silica glass has tensile strength >5 GPa [30]. Taken into account such value, it would suggest that large area can be fabricated when the number of layer is above 3, while the system needs to be carefully assessed in the case of a single layer. Again, as the FOM increase with the number of layer, the acceleration times increase to 4912 s and 491 s for a N=3 structure, for powers of 10 GW and 100 GW respectively.

Another critical aspect is the ability of properly control the lightsail's direction during acceleration. Different solutions have been proposed, among which the use of a tailored laser beam intensity to trap the sail [15], which will be very suitable for this type of solution.

Lastly, in case the sail must need to survive along the entire journey, for instance to be used for communication purposes, the space environmental effects have to be taken into

account. In fact, the spacecraft would experience the interaction with interstellar gas and dust in the interstellar medium (ISM). Most of the ISM consists of gaseous matter, approximately 99% of the total mass, while the remaining part is composed of granular dust. Of the gaseous matter, approximately 98% consists of hydrogen (70%) and helium (28%), and the remaining 2% includes heavier elements such as carbon, oxygen and iron [31, 32]. A theoretical study has been carried out to investigate the damage induced by various agents during a relativistic journey [33]; nevertheless the gas accumulation effect in materials that propagates at relativistic speed is still rather unexplored [34, 35]. Depending on energy, ions are expected to implant at different depth in the materials, potentially causing serious damages in the lightsail. A collection of experiments carried out on virgin and protected mirrors have been reported [36, 37, 38, 39, 40, 41, 42], even though much work still needs to be done to model and prove lightsail hardness.

5 Conclusions

Thin film multilayers in the sub-micrometric scale could be a valuable solution for realizing low mass DE accelerated lightsails. Different optimized structures have been proposed to maximize the propulsion efficiency, which depends on the reflectance and absorption of the ligthsail in the Doppler-shifted wavelength region of the laser source, and on the areal density of the lightsail itself. The proposed solutions have been analyzed in order to verify their thermal stability during the acceleration phase, which results as the ultimate criteria to assess their suitability. The most promising structures to be used with a 1064 laser source result to be the TiO_2-based ones, in the form of single layer or multilayer stack which include the SiO_2 as a second material. In term of propulsion efficiency, the single layer results to be the most performing, while the multilayers offer some advantages in term of thermal control and stiffness. Engineering process is fundamental to obtain proper optical characteristic, thus reducing the absorption of the lightsail in the Doppler-shifted wavelength of the laser in order to allow the use of high power laser up to 100 GW. The use of longer wavelength a laser source could expand the choice of potential materials having the required optical characteristics.

Acknowledgements

PML funding for this program comes from NASA grants NIAC Phase I DEEP-IN – 2015 NNX15AL91G and NASA NIAC Phase II DEIS – 2016 NNX16AL32G and the NASA California Space Grant NASA NNX10AT93H as well as a generous gift from the Emmett and Gladys W. Fund for the Starlight program and from the Breakthrough Initiatives Foundation for the Starshot program.

Author contributions

G.S. developed the mathematical code and carried out all the simulations; he draft some parts of the paper. G.F. conceived the thermal analysis, contributed to simulations and draft some parts of the paper. A.J.C. coordinated the mathematical modeling, wrote the paper and contributed to its finalization. P.L. provided insightful ideas and inputs, as well as valuable feedback. R.R., M.B. and D.G. contributed with fruitful scientific discussions. M.G.P. conceived the paper scientific idea, coordinated the scientific activities and simulations, wrote the paper and finalize it. All authors reviewed the final manuscript.

References

[1] Y. Tsuda, O. Mori, R. Funase, H. Sawada, T. Yamamoto, T. Saiki, T. Endo, and J. Kawaguchi. Flight status of ikaros deep space solar sail demonstrator. *Acta astronautica*, 69(9-10):833–840, 2011.

[2] Igor Levchenko, Kateryna Bazaka, Stephane Mazouffre, and Shuyan Xu. Prospects and physical mechanisms for photonic space propulsion. *Nature Photonics*, 12:649–657, 2018.

[3] L. Felicetti and F. Santoni. Nanosatellite swarm missions in low earth orbit using laser propulsion. *Aerospace Science and Technology*, 27(1):179–187, 2013.

[4] C. Phipps, M. Birkan, W. Bohn, H.-A. Eckel, H. Horisawa, T. Lippert, M. Michaelis, Y. Rezunkov, A. Sasoh, W. Schall, S. Scharring, and J. Sinko. Review: Laser-ablation propulsion. *Journal of Propulsion and Power*, 26(4):609–637, 2010.

[5] G. Marx. Interstellar vehicle propelled by terrestrial laser beam. *Nature*, 211(5044):22–23, 1966.

[6] R. L. Forward. Roundtrip interstellar travel using laser-pushed lightsails. *Journal of Spacecraft and Rockets*, 21(2):187–195, 1984.

[7] P. Lubin. A roadmap to interstellar flight. *JBIS - Journal of the British Interplanetary Society*, 69(2-3):40–72, 2016.

[8] Neeraj Kulkarni, Philip Lubin, and Qicheng Zhang. Relativistic spacecraft propelled by directed energy. *The Astronomical Journal*, 155(4):155, 2018.

[9] P. Lubin and W. Hettel. The path to interstellar flight. *Acta Futura*, 12(9):9–44, 2020.

[10] Chang H. Wu Y. Xiao P. Yi N. Lu Y. Ma Y. Huang Y. Zhao K. Yan X.Q. Zhang, T. and Z.B. Liu. Nanosatellite swarm missions in low earth orbit using laser propulsion. *Nature Photonics*, 9(7):471–476, 2015.

[11] Todd F. Sheerin, Elaine Petro, Kelley Winters, Paulo Lozano, and Philip Lubin. Fast solar system transportation with electric propulsion powered by directed energy. *Acta Astronautica*, 179:78–87, 2021.

[12] Shatligth. *https://www.deepspace.ucsb.edu/projects/starlight*, 2021.

[13] Brekthrough starshot. *https://breakthroughinitiatives.org/initiative/3*, 2021.

[14] Ognjen Ilic, Cora M. Went, and Harry A. Atwater. Nanophotonic heterostructures for efficient propulsion and radiative cooling of relativistic light sails. *Nano Letters*, 18(9):5583–5589, 2018.

[15] Harry A. Atwater, Artur R. Davoyan, Ognjen Ilic, Deep Jariwala, Michelle C. Sherrott, Cora M. Went, William S. Whitney, and Joeson Wong. Materials challenges for the starshot lightsail. *Nature Materials*, 17:861–867, 2018.

[16] R. Kitamura, L. Pilon, and M. Jonasz. Optical constants of silica glass from extreme ultraviolet to far infrared at near room temperature. *Appl. Opt.*, 46(33):8118–8133, 2007.

[17] Rémi Boidin, Tomáš Halenkovič, Virginie Nazabal, Ludvík Beneš, and Petr Němec. Pulsed laser deposited alumina thin films. *Ceramics International*, 42(1):1177–1182, 2016.

[18] Thomas Siefke, Stefanie Kroker, Kristin Pfeiffer, Oliver Puffky, Kay Dietrich, Daniel Franta, Ivan Ohlídal, Adriana Szeghalmi, Ernst-Bernhard Kley, and Andreas Tünnermann. Materials pushing the application limits of wire grid polarizers further into the deep ultraviolet spectral range. *Advanced Optical Materials*, 4(11):1780–1786, 2016.

[19] Juan I. Larruquert, Antonio P. Pérez-Marín, Sergio García-Cortés, Luis Rodríguez de Marcos, José A. Aznárez, and José A. Méndez. Self-consistent optical constants of sic thin films. *J. Opt. Soc. Am. A*, 28(11):2340–2345, 2011.

[20] D. T. Pierce and W. E. Spicer. Electronic structure of amorphous si from photoemission and optical studies. *Phys. Rev. B*, 5:3017–3029, 1972.

[21] Martin A. Green. Self-consistent optical parameters of intrinsic silicon at 300k including temperature coefficients. *Solar Energy Materials and Solar Cells*, 92(11):1305–1310, 2008.

[22] Luis V. Rodríguez de Marcos, Juan I. Larruquert, José A. Méndez, and José A. Aznárez. Self-consistent optical constants of mgf2, laf3, and cef3 films. *Opt. Mater. Express*, 7(3):989–1006, 2017.

[23] J. Yao, J. Ma, C. Xiu, Z. Fan, Y. Jin, Y. Zhao, H. He, J. Shao, H. Huang, F. Zhang, and Z. Wu. Laser-induced damage of TiO2SiO2 high reflector at 1064nm. *Journal of Applied Physics*, 103(8):83–103, 2008.

[24] M. R. Querry. Optical constants. Missouri Univ-Kansas City., 1985.

[25] Carsten Schinke, P. Christian Peest, Jan Schmidt, Rolf Brendel, Karsten Bothe, Malte R. Vogt, Ingo Kröger, Stefan Winter, Alfred Schirmacher, Siew Lim, Hieu T. Nguyen, and Daniel MacDonald. Uncertainty analysis for the coefficient of band-to-band absorption of crystalline silicon. *AIP Advances*, 5(6):067168, 2015.

[26] Yongshuai Xie, Lin Wang, Ying Peng, Dehua Ma, Luyi Zhu, Guanghui Zhang, and Xinqiang Wang. High temperature and high strength Y2Zr2O7 flexible fibrous membrane for efficient heat insulation and acoustic absorption. *Chemical Engineering Journal*, 416:128994, 2021.

[27] Yongshuai Xie, Ying Peng, Dehua Ma, Wei Liu, Zhezhe Deng, Luyi Zhu, Guanghui Zhang, and Xinqiang Wang. Lightweight, high-strength, flexible YAG fibrous membrane for efficient heat insulation. *Journal of Alloys and Compounds*, 876:159978, 2021.

[28] C. Burger, B. S. Hsiao, and B. Chu. Nanofibrous materials and their applications. *Annu. Rev. Mater. Res.*, 36:333–368, 2006.

[29] S.R.J Saunders and H.R Vetters. Standardisation of test methods for the mechanical properties of thin coatings. *Thin Solid Films*, 299(1):82–87, 1997.

[30] G Scott Glaesemann. Optical fiber mechanical reliability. *White Paper*, 8002:1–62, 2017.

[31] Ralf S Klessen and Simon CO Glover. Physical processes in the interstellar medium. In *Star Formation in Galaxy Evolution: Connecting Numerical Models to Reality*, pages 85–249. Springer, 2016.

[32] B. T. Draine. *Physics of the interstellar and intergalactic medium*, volume 19. Princeton University Press, 2010.

[33] Thiem Hoang, A. Lazarian, Blakesley Burkhart, and Abraham Loeb. The interaction of relativistic spacecrafts with the interstellar medium. *The Astrophysical Journal*, 837(1):5, 2017.

[34] Jon Drobny, Alexander N. Cohen, Davide Curreli, Philip Lubin, Maria G. Pelizzo, and Maxim Umansky. Damage to Relativistic Interstellar Spacecraft by ISM Impact Gas Accumulation. *The American Astronomical Society*, 908(2):248, 2021.

[35] Jon Drobny, Alexander N Cohen, Davide Curreli, Philip Lubin, Maria G Pelizzo, and Maxim Umansky. Survivability of metallic shields for relativistic spacecraft. *JBIS-Journal of the British Interplanetary Society*, 73(12):446–456, 2020.

[36] W. Wang, J. Roth, S. Lindig, and C. H. Wu. Blister formation of tungsten due to ion bombardment. *Journal of nuclear materials*, 299(2):124–131, 2001.

[37] M.G. Pelizzo, A.J. Corso, P. Zuppella, D.L. Windt, G. Mattei, and P. Nicolosi. Stability of extreme ultraviolet multilayer coatings to low energy proton bombardment. *Opt. Express*, 19(16):14838–14844, 2011.

[38] MG Pelizzo, AJ Corso, E Tessarolo, R Bottger, R Hubner, E Napolitani, M Bazzan, M Rancan, L Armelao, W Jark, et al. Morphological and functional modifications of optical thin films for space applications irradiated with low-energy helium ions. *ACS applied materials & interfaces*, 10(40):34781–34791, 2018.

[39] R. Livengood, S. Tan, Y. Greenzweig, J. Notte, and S. McVey. Subsurface damage from helium ions as a function of dose, beam energy, and dose rate. *Journal of Vacuum Science & Technology B: Microelectronics and Nanometer Structures Processing, Measurement, and Phenomena*, 27(6):3244–3249, 2009.

[40] Denis Garoli, Luis V. Rodriguez De Marcos, Juan I. Larruquert, Alain J. Corso, Remo Proietti Zaccaria, and Maria G. Pelizzo. Mirrors for space telescopes: Degradation issues. *Applied Sciences*, 10(21), 2020.

[41] Sara Zuccon, Enrico Napolitani, Enrico Tessarolo, Paola Zuppella, Alain J Corso, F Gerlin, M Nardello, and Maria G Pelizzo. Effects of helium ion bombardment on metallic gold and iridium thin films. *Optical Materials Express*, 5(1):176–187, 2015.

[42] Maria G Pelizzo, Alain J Corso, Giovanni Santi, René Hübner, Denis Garoli, Dominic Doyle, Philip Lubin, Alexander N Cohen, Jacob Erlikhman, Giulio Favaro, et al. Dependence of the damage in optical metal/dielectric coatings on the energy of ions in irradiation experiments for space qualification. *Scientific reports*, 11:1–12, 2021.

Supplementary Files

This is a list of supplementary files associated with this preprint. Click to download.

- papermultilayerlightsailsupplementary.pdf